

# Magnetization cusp singularities of frustrated Kondo necklace model

Takahiro Yamamoto, Rumi Manago, and Yoshihiro Mori  
*Department of Physics, Faculty of Science, Tokyo University of Science,  
 1-3 Kagurazaka, Shinjuku-ku, Tokyo 162-8601, Japan*

(Dated:)

We present a detailed study of the magnetization process of frustrated Kondo necklace model by means of analytical and numerical techniques. The density matrix renormalization group (DMRG) calculations find two plateaus and two cusps in the magnetization curves. The magnetization plateaus at zero ( $m = 0$ ) and at a half saturation magnetization ( $m = 1/2$ ) were previously found by numerical exact-diagonalization, and these mechanisms were well understood. The two magnetization cusps appears in the low-field ( $0 < m < 1/2$ ) and high-field ( $1/2 < m < 1$ ) regions respectively. Of these two cusps, the high-field cusp was expected from the study of a frustrated one-dimensional spin chain, but the low-field cusp was unexpected. We therefore focus on the cusp in the low-field region, where the degree of freedom of innercore spins is active. We use a fermionic bond-operator representation to discuss the magnetization cusp. The appearance of the cusp can be understood in terms of the energy dispersion with double bottoms obtained from a strong Kondo-coupling expansion. We also discuss the critical behavior of the magnetization near the cusp singularity and find that  $m - m_{\text{cusp}} \propto -\sqrt{h_{\text{cusp}} - h}$  ( $h < h_{\text{cusp}}$ ) and  $m - m_{\text{cusp}} \propto h - h_{\text{cusp}}$  ( $h > h_{\text{cusp}}$ ). We further obtain the phase diagram showing whether the cusp appears in the magnetization curve.

PACS numbers: 75.10.Jm, 75.20Hr, 75.30.Kz

## I. INTRODUCTION

Recently, effects of the frustrations for low-dimensional quantum spin systems have attracted much attention and have been extensively studied theoretically and experimentally. The competition between the frustration and quantum fluctuations may give rise to quantum phase transitions, not only in the absence of an external magnetic field but also in the finite field. Interests in the field-induced quantum phase transitions arising from this competition have been growing for the last several years (e.g. magnetization plateaus [1, 2, 3, 4, 5, 6], cusp singularities [7, 8, 9, 10, 11] and spin-flopping phenomena [12, 13]).

In recent papers [14, 15, 16], we studied the magnetization process of the frustrated Kondo necklace model using a finite size scaling analysis of the exact diagonalization data. The Hamiltonian of the Kondo necklace model in a uniform magnetic field is given by

$$\mathcal{H} = J \sum_{j=1}^L (\boldsymbol{\sigma}_j \cdot \boldsymbol{\sigma}_{j+1} + \lambda \boldsymbol{\sigma}_j \cdot \boldsymbol{\sigma}_{j+2}) + J_K \sum_{j=1}^L \boldsymbol{\sigma}_j \cdot \mathbf{S}_j - h \sum_{j=1}^L (\sigma_j^z + S_j^z). \quad (1)$$

Here  $\boldsymbol{\sigma}_j$  and  $\mathbf{S}_j$  are spin-1/2 operators of the conduction and the innercore electrons on the  $j$ -th site ( $1 \leq j \leq L$ ), respectively.  $h$  is a rescaled magnetic field including the  $g$ -factor and Bohr magneton  $\mu_B$ . The Kondo exchange coupling  $J_K$  is antiferromagnetic ( $J_K > 0$ ). In the case of the ferromagnetic Kondo coupling ( $J_K < 0$ ), this model Eq. (1) has a connection with Haldane problem[17]. Henceforth, the Kondo coupling  $J_K$  is taken as unit of energy (i.e., we take  $J_K = 1$ ).

The Kondo necklace model without the frustration ( $\lambda = 0$ ) was originally introduced by Doniach, [18] in order to describe the competition between the intra-atomic Kondo coupling and inter-atomic Ruderman-Kittel-Kasuya-Yosida (RKKY) interaction in the heavy electron systems. The Kondo coupling favors the formation of intra-atomic quantum disorder (Kondo singlet) phase, while the RKKY interaction tends to induce an antiferromagnetic ordered phase. In one-dimensional system, however, the Kondo singlet phase is stabilized and the gap  $\Delta_K$  characterizing this phase is opened for any finite Kondo coupling [19, 20, 21, 22, 23]. Thus, the magnetization of this system appears only above a critical magnetic field  $h > h_c = \Delta_K$ . In the absence of the frustration ( $\lambda = 0$ ), the magnetization increases smoothly with increasing external magnetic field up to the saturation field  $h_S$ , indicating no quantum phase transition in the region  $\Delta_K < h < h_S$ .

When we turn on the frustration, the frustrated Kondo necklace model in Eq. (1) exhibits a plateau at a half the saturation magnetization ( $m = 1/2$ ) in addition to the plateau at  $m = 0$ . Our previous study [15, 16] made it clear that the system with  $m = 1/2$  can be effectively regarded as spin-1/2 XXZ model with next-nearest-neighbor interactions (so-called spin-1/2 zig-zag ladder) because innercore  $S$ -spins are almost ferromagnetically ordered along a direction of the magnetic field and degree of freedom of  $S$ -spins is frozen in this region. Thus, the magnetization plateau at  $m = 1/2$  can be understood as the  $\sigma$ -dimer gap with broken translational symmetry, and we can expect that the magnetization growth from the plateau is essentially equivalent to that of the spin-1/2 zig-zag ladder. Recently, Okunishi et al. [10] studied the magnetization curve of the spin-1/2 zig-zag ladder using the product-wave function renormalization group (PWFRG) method, which is

a variant of the density-matrix renormalization group (DMRG) method [24]. They found a cusp-type singularity in the magnetization curve, and explained its appearance in terms of the double-bottom shape of the single-magnon energy dispersion.

As we mentioned above, there is a result of Ref. [10] led us to a prediction that the cusp should also appears in the magnetization curve in the high-field region ( $1/2 < m < 1$ ) in our model. Stimulated by Ref. [10], to detect weak singularities like the cusp, we calculate again the magnetization curve of the frustrated Kondo necklace model with use of the DMRG method which is one of the most suitable numerical method for treating low-dimensional many-body systems. As we show in the next section, our DMRG calculations clearly find the cusp in high-field region according to our expectation and besides unexpected cusp-type singularity in the low-field region ( $0 < m < 1/2$ ). In the low-field region, since the degree of freedom of the innercore spins is active, we cannot explain appearance of the cusp making use of above-mentioned single-magnon picture which is effective in the high-field region. Therefore, new picture describing low-energy excitations from the Kondo singlet phase will be required.

This paper is organized as follows. In Sec.II, we show the DMRG results of the magnetization curves of the frustrated Kondo necklace model. In Sec.III, the frustrated Kondo necklace model is described in terms of four types of interaction fermions, corresponding to singlet and three triplet states (Sec.III A), and a mechanism of appearance of the low-field cusp is explained in terms of the double-bottom shape of low-energy dispersion obtained by strong Kondo-coupling expansion (Sec.III B). In Sec.IV, we will also discuss critical behavior of the magnetization near the cusp singularity point in the low-field region ( $0 < m < 1/2$ ). In Sec.V, we will show the phase diagram on  $J$ - $\lambda$  plane which decides whether the cusp singularity appears in the magnetization curve or not. The final section (Sec.VI) is devoted to summary and discussion.

## II. MAGNETIZATION CURVES

We used DMRG method based on the finite-size algorithm to obtain the ground-state magnetization curves of the frustrated Kondo necklace model. Our DMRG calculations have been performed under the open boundary condition, with the system length  $L = 60$  and the truncation number up to 120.

Figure 1 shows the magnetization curves for fixed  $J = 1.0$  with  $\lambda = 0.0$  and  $0.5$ . In the absence of frustration ( $\lambda = 0.0$ ), the magnetization curve smoothly grows with increasing magnetic field  $h$  after the Kondo singlet gap collapses. This means that there is no field-induced quantum phase transition in the region  $\Delta_K < h < h_S$ .

In contrast, in the case of  $\lambda = 0.5$ , we confirm again that two plateaus appear at zero ( $m = 0$ ) and a half sat-

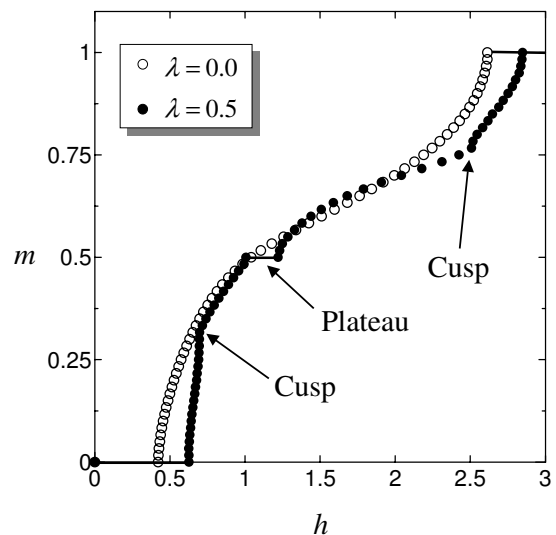


FIG. 1: The magnetization curves of frustrated Kondo necklace model with  $J = 1.0$  for  $\lambda = 0.0$  and  $0.5$ .

uration ( $m = 1/2$ ) magnetizations was previously found by exact-diagonalization method. As is known in our previous papers, [14, 15, 16] the spin configuration at the plateau represents the doubly degenerate  $\sigma$ -dimer states with broken translational symmetry. Moreover, our DMRG calculations find two cusp singularities which cannot be detected by the exact-diagonalization calculations. As we mentioned in Sec.I, although a high-field cusp in the region  $1/2 < m < 1$  was expected from the results of Ref. [10], the low-field cusp in the region  $0 < m < 1/2$  was unexpected. Therefore, the high-field cusp can be interpreted in terms of the low-energy dispersion with double-bottom shape of single down-spin magnon in Ref. [10]. However, this single-magnon picture is only valid in the high-field region, and cannot be used to explain the cusp in the low-field region  $0 < m < 1/2$ . To discuss the low-field cusp, we must consider elementary excitations involving the degree of freedom of the innercore spins. Thus, we are mainly interested in the cusp appearing in the region  $0 < m < 1/2$ .

In next section, we give an interpretation for the cusp in  $0 < m < 1/2$ . In Sec.IV, we will also show the phase diagram on  $J$ - $\lambda$  plane which decides whether the cusp singularity appears in the magnetization curve or not.

## III. LOW-FIELD CUSP SINGULARITY

### A. Fermionic bond-operator representation

In this section, we use a bond-operator representation of the frustrated Kondo necklace model and clarify the mechanism of the appearance of the cusp in the region  $0 < m < 1/2$ . Since the ground state in the absence of the magnetic field is an aggregate of intra-atomic

Kondo singlets, the low-energy physics can be described by triplet excitations from the Kondo singlet sea. To express this picture explicitly, we introduce the bond-operators:

$$|s\rangle = s^\dagger |\text{vac}\rangle = \frac{1}{\sqrt{2}} (|\uparrow\downarrow\rangle - |\downarrow\uparrow\rangle), \quad (2)$$

$$|t_x\rangle = t_x^\dagger |\text{vac}\rangle = -\frac{1}{\sqrt{2}} (|\uparrow\uparrow\rangle - |\downarrow\downarrow\rangle), \quad (3)$$

$$|t_y\rangle = t_y^\dagger |\text{vac}\rangle = \frac{i}{\sqrt{2}} (|\uparrow\uparrow\rangle + |\downarrow\downarrow\rangle), \quad (4)$$

$$|t_z\rangle = t_z^\dagger |\text{vac}\rangle = \frac{1}{\sqrt{2}} (|\uparrow\downarrow\rangle + |\downarrow\uparrow\rangle), \quad (5)$$

which were first proposed by Sachdev and Bhatt [25]. Here,  $\uparrow, \downarrow$  and  $\uparrow, \downarrow$  denote  $z$ -components of  $\sigma$ - and  $S$ -spins, and  $|\text{vac}\rangle$  is the vacuum state. As we show below,  $s$  and  $t_\alpha$  ( $\alpha = x, y, z$ ) can be either fermionic or bosonic.

Clearly only one of these new particles can occupy each site. Therefore, in order to restrict the physical subspace with single particle on each site, one must impose a local constraint on the number operator of these particles

$$s_j^\dagger s_j + \sum_{\alpha=x,y,z} t_{\alpha,j}^\dagger t_{\alpha,j} = 1. \quad (6)$$

The  $\sigma$ - and  $S$ -spins are represented in terms of these new operators as

$$\sigma_j^\alpha = \frac{1}{2} \left( -s_j^\dagger t_{\alpha,j} - t_{\alpha,j}^\dagger s_j - i\epsilon_{\alpha\beta\gamma} t_{\beta,j}^\dagger t_{\gamma,j} \right), \quad (7)$$

$$S_j^\alpha = \frac{1}{2} \left( s_j^\dagger t_{\alpha,j} + t_{\alpha,j}^\dagger s_j - i\epsilon_{\alpha\beta\gamma} t_{\beta,j}^\dagger t_{\gamma,j} \right), \quad (8)$$

where  $\epsilon_{\alpha\beta\gamma}$  is the antisymmetric Levi-Civita tensor. Henceforth, it is promised that all repeated indices  $\alpha$ ,  $\beta$  and  $\gamma$  are summed over  $x, y$  and  $z$ .

Thus far we have not specified the algebra of the singlet ( $s^\dagger$ ) and triplet ( $t^\dagger$ ) operators. If the singlet and triplet operators at each site satisfy either bosonic commutation or fermionic anticommutation relations, the spin algebra

$$\begin{aligned} [\sigma_j^\alpha, \sigma_j^\beta] &= i\epsilon_{\alpha\beta\gamma} \sigma_j^\gamma, & [S_j^\alpha, S_j^\beta] &= i\epsilon_{\alpha\beta\gamma} S_j^\gamma, \\ [\sigma_j^\alpha, S_j^\beta] &= 0, & \sigma_j^2 = S_j^2 &= \frac{1}{2} \left( \frac{1}{2} + 1 \right) \end{aligned} \quad (9)$$

can be easily obtained by using the expressions Eq.(7) and Eq.(8). The algebra of bond-operators is usually chosen as bosonic one to perform a physically meaningful mean-field theory based on an idea of Bose-Einstein condensation of singlet states,  $\langle s \rangle = \langle s^\dagger \rangle \neq 0$ ,  $\langle t \rangle = \langle t^\dagger \rangle = 0$ . The bosonic mean-field theory was successfully applied to study the properties of disordered dimerized phases in many quantum spin systems (e.g. spin-1/2 ladder [26], Bilayer Heisenberg model [27], and standard Kondo necklace model [19]). Recently, using the bosonic bond-operators, magnetization process of the spin-1 chain and spin-1/2 and spin-1 ladders were *undirectly* studied by mapping onto effective Hamiltonian of  $S = 1/2$  pseudospins in the effective magnetic field [28].

However, in this paper, we choose the fermionic anticommutation relations

$$\{s_j, s_j^\dagger\} = 1, \quad \{t_{\alpha,j}, t_{\beta,j}^\dagger\} = \delta_{\alpha,\beta}, \quad \{s_j, t_{\alpha,j}^\dagger\} = 0, \quad (10)$$

which is more convenient to *directly* discuss the magnetization growth. Using the fermionic bond-operator expression, the Hamiltonian Eq.(1) is written as

$$\mathcal{H} = \mathcal{H}_0 + \sum_{\nu=1,2} \lambda^{\nu-1} \left( \mathcal{H}_1^{(\nu)} + \mathcal{H}_2^{(\nu)} + \mathcal{H}_3^{(\nu)} \right), \quad (11)$$

where each part is expressed as

$$\mathcal{H}_0 = \sum_{j=1}^L \left( -\frac{3}{4} s_j^\dagger s_j + \frac{1}{4} t_{\alpha,j}^\dagger t_{\alpha,j} \right) - \mu \sum_{j=1}^L \left( s_j^\dagger s_j + t_{\alpha,j}^\dagger t_{\alpha,j} - 1 \right), \quad (12a)$$

$$\mathcal{H}_1^{(\nu)} = -\frac{J}{4} \sum_{j=1}^L \left[ s_j^\dagger s_{j+\nu}^\dagger t_{\alpha,j} t_{\alpha,j+\nu} + s_j^\dagger t_{\alpha,j+\nu}^\dagger t_{\alpha,j} s_{j+\nu} + \text{h.c.} \right], \quad (12b)$$

$$\mathcal{H}_2^{(\nu)} = -\frac{J}{4} \sum_{j=1}^L \epsilon_{\alpha\beta\gamma} \left[ i \left( s_j^\dagger t_{\beta,j+\nu}^\dagger t_{\alpha,j} t_{\gamma,j+\nu} + t_{\beta,j}^\dagger s_{j+\nu}^\dagger t_{\gamma,j} t_{\alpha,j+\nu} \right) + \text{h.c.} \right], \quad (12c)$$

$$\mathcal{H}_3^{(\nu)} = \frac{J}{8} \sum_{j=1}^L \left[ (1 - \delta_{\alpha,\beta}) \left( t_{\alpha,j}^\dagger t_{\alpha,j+\nu}^\dagger t_{\beta,j} t_{\beta,j+\nu} - t_{\alpha,j}^\dagger t_{\beta,j+\nu}^\dagger t_{\beta,j} t_{\alpha,j+\nu} \right) + \text{h.c.} \right]. \quad (12d)$$

$\mathcal{H}_1^{(\nu)}$  describes the couplings between the singlet and triplet fermions, and  $\mathcal{H}_2^{(\nu)}$  shows the couplings of one

singlet and three different triplets.  $\mathcal{H}_3^{(\nu)}$  describes the scatterings between the triplets. We have also introduced

local chemical potentials  $\mu_j$  to impose the local constraint (6) and replaced  $\mu_j$  by a global one  $\mu$  in accordance with the translational symmetry of original Hamiltonian along the chain axis. The replacement is reasonable procedure to explain the magnetization cusp, which is a phase transition without broken translational symmetry. In contrast, the plateau state with the broken symmetry cannot be explained by this treatment.

Next, we introduce new two fermionic operators  $t_+$  and  $t_-$  corresponding to the two states  $|\uparrow\uparrow\rangle$  and  $|\downarrow\downarrow\rangle$  instead of the transverse triplet operators  $t_x$  and  $t_y$ :

$$|\uparrow\uparrow\rangle = t_+^\dagger |\text{vac}\rangle = \frac{-1}{\sqrt{2}} (t_x^\dagger + it_y^\dagger) |\text{vac}\rangle, \quad (13)$$

$$|\downarrow\downarrow\rangle = t_-^\dagger |\text{vac}\rangle = \frac{1}{\sqrt{2}} (t_x^\dagger - it_y^\dagger) |\text{vac}\rangle. \quad (14)$$

These expressions are more convenient to discuss the magnetization process. It is straightforward to write the Hamiltonian (12a)-(12d) using the new operators  $t_+$  and  $t_-$  defined by Eqs.(13) and (14). The new expression makes it easy to perform perturbation expansion given in the next section, although it looks more complicated than the expressions (12a)-(12d).

Finally, the Zeeman energy in this expression is given by

$$\mathcal{H}_{\text{Zeeman}} = -h \sum_{j=1}^L (t_{+,j}^\dagger t_{+,j} - t_{-,j}^\dagger t_{-,j}), \quad (15)$$

where  $\sum_{j=1}^L (t_{+,j}^\dagger t_{+,j} - t_{-,j}^\dagger t_{-,j})$  corresponds to a total magnetization  $\sum_{j=1}^L (\sigma_j^z + S_j^z)$  and the magnetic field  $h$  fills the role of the Fermi energy for the triplet particles.

## B. Strong Kondo-coupling expansion

In this subsection, we carry out a strong Kondo-coupling expansion in order to clarify how the cusp singularity appears in the magnetization curve in the present model. First, let us consider the ground state in the strong Kondo-coupling limit  $J \ll J_K = 1$ . In this limit, the Kondo coupling Hamiltonian  $\mathcal{H}_0$  will be treated as the unperturbed one and its ground state is a direct product of intra-atomic Kondo singlets

$$|0\rangle = s_1^\dagger s_2^\dagger \cdots s_L^\dagger |\text{vac}\rangle \quad (16)$$

with the energy  $\langle 0 | \mathcal{H}_0 | 0 \rangle = -3L/4$ . On the other hand, the intra-chain Hamiltonians  $\mathcal{H}_1^{(\nu)}$ ,  $\mathcal{H}_2^{(\nu)}$  and  $\mathcal{H}_3^{(\nu)}$  will be treated as the perturbation. The first-order perturbation energy vanishes due to the orthogonal condition. The second-order correction to the ground-state energy is calculated by the standard perturbation formula. The perturbation energy up to second order in  $J$  is obtained as

$$E_0 = L \left\{ -\frac{3}{4} - \frac{3}{16} (1 + \lambda^2) J^2 \right\}. \quad (17)$$

To obtain the low-energy spectrum, we next study the energy correction in an excited state. We suppose that the low-energy physics in the strong Kondo-coupling region is described by single triplet excitation states propagating as a plane wave in the singlet sea [29],

$$|k\rangle = \frac{1}{\sqrt{L}} \sum_{j=1}^L \exp(ikj) s_1^\dagger s_2^\dagger \cdots t_{+,j}^\dagger \cdots s_L^\dagger |\text{vac}\rangle. \quad (18)$$

This wavefunction satisfies the constraint Eq.(6). Here, we neglect other two triplet states with total magnetization  $M = 0$  and  $-1$  under the magnetic field. We note that the states described by Eq.(18) have a translational symmetry. This is consistent with the replacement of the local chemical potential  $\mu_j$  by global one  $\mu$ . Following the same procedure as calculating the ground-state energy, we can estimate the excitation energy using the wave-function given by Eq.(18). The result is given by

$$\begin{aligned} E_k = & \left( -\frac{3}{4}L + 1 \right) + \frac{J}{2} (\cos k + \lambda \cos(2k)) \\ & - \frac{1}{32} J^2 \{ (1 + \lambda^2)(3L + 2) - 4(2 - \lambda) \cos(k) \\ & + 2(1 - 4\lambda^2) \cos(2k) + 4\lambda \cos(3k) + 2\lambda^2 \cos(4k) \}, \end{aligned} \quad (19)$$

which is independent of  $\alpha$ . The Hamiltonian  $\mathcal{H}_3^{(\nu)}$  indicating the scatterings between triplets has no contribution to the single triplet energy (19), because the states (18) include only a single triplet fermion.

Subtracting Eq.(17) from Eq.(19), we find the single triplet excitation spectrum to second order in  $J$ :

$$\begin{aligned} \omega(k) & \equiv E_k - E_0 \\ & = 1 - \frac{1}{16} (1 + \lambda^2) J^2 + \frac{1}{8} \{ 4 + (2 - \lambda)J \} J \cos k \\ & \quad + \frac{1}{16} \{ 8\lambda - (1 - 4\lambda^2)J \} J \cos(2k) \\ & \quad - \frac{1}{8} \lambda J^2 \cos(3k) - \left( \frac{\lambda J}{4} \right)^2 \cos(4k), \end{aligned} \quad (20)$$

which is an even function of  $k$  around  $k = \pi$ . As a typical example, in Fig.2, we plot the energy dispersion for  $J = 0.1$  with  $\lambda = 0.2$  and  $0.4$  by solid line.

To show the validity of these analytical results based on the strong Kondo-coupling expansion, we also calculate the energy dispersions using the exact-diagonalization under the periodic boundary condition ( $\sigma_j = \sigma_{j+L}$  and  $S_j = S_{j+L}$ ). Here we briefly describe our diagonalization method. Since the  $z$ -component of total spin operator commutes with the frustrated Kondo necklace Hamiltonian (1), all eigenvalues and eigenstates of the Hamiltonian are labeled by the total magnetization  $M$  is eigenvalue of  $\sum_{j=1}^L (\sigma_j^z + S_j^z)$ . In addition, since the Hamiltonian (1) is invariant under the translation along the chain-direction ( $\sigma_j \rightarrow \sigma_{j+1}$  and  $S_j \rightarrow S_{j+L}$ ), the eigenvalues and eigenstates are classified by the wave number  $k = 2\pi n/L$  ( $n = 0, 1, \dots, L-1$ ) corresponding to

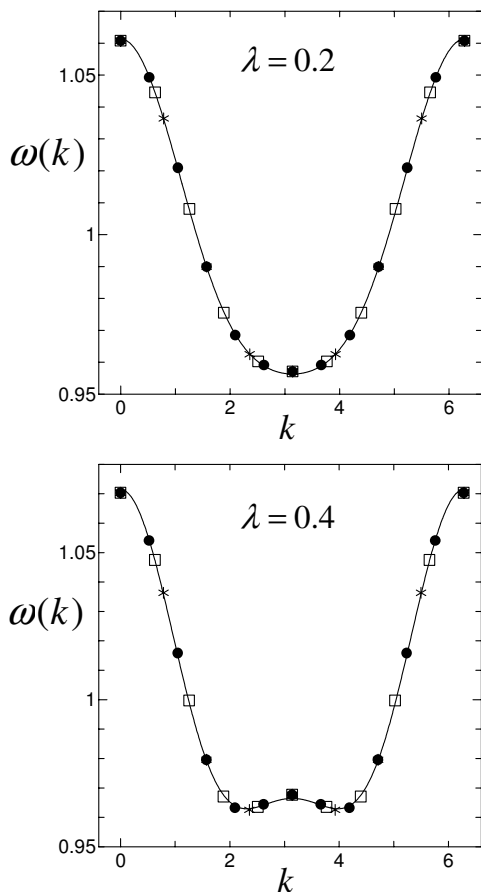


FIG. 2: The energy dispersion of a single triplet fermion for  $\lambda = 0.2$  (above) and  $0.4$  (below). Solid lines represent the dispersion obtained by the strong Kondo-coupling expansion. The asterisks, open squares and filled circles show the gap between singlet and triplet states at  $k = 2\pi n/L$  ( $n = 0, 1, \dots, L-1$ ) for  $L = 8, 10$  and  $12$  respectively, which are obtained by the exact-diagonalization method.

eigenvalue of the translation operator. Thus, we calculate the lowest energy  $E(k, M)$  in the subspace specified by  $M$  and  $k$ . In Fig.2, we plot the singlet-triplet gaps  $E(k, M=1) - E(k, M=0)$  for finite length  $L = 8$  (asterisk),  $10$  (square) and  $12$  (circle).

As the figure indicates, the results of the strong Kondo-coupling expansion (solid lines) are in good quantitative agreement with the exact-diagonalization data. This means that low-energy phenomena in this system is well described by the single triplet state  $|k\rangle$  described by Eq.(18), although the state (18) is not eigenstate of the Hamiltonian  $\mathcal{H}$ .

The shape of  $\omega(k)$  for  $\lambda = 0.2$  and  $0.4$  are qualitatively different from each other. The former has a single bottom (minima) at  $k = \pi$ , while the latter has a double-bottom shape. From Fig.2, we can provide a qualitative explanation based on the single particle band-picture for appearance of cusp singularity in the magnetization curve.

When the magnetic field is applied in the system, the states below the Fermi energy ( $\omega(k) < h$ ) are occupied by the  $t_+$  particles. Thus, the magnetization of the system is given by the total number of  $t_+$  particles occupying the energy lower than the Fermi energy  $h$ , namely

$$m = \frac{1}{2\pi} \int_0^{2\pi} \theta(h - \omega(k)) dk, \quad (21)$$

where  $\theta(x)$  is the Heaviside's step function. Therefore, in the case of the dispersion with double bottoms, the increase ratio of the particle number drastically changes when the Fermi energy  $h$  reaches the local maximum  $h_{\text{cusp}} = \omega(\pi)$ . The drastic change of the increase ratio is an origin of appearance of the cusp singularity. In next section, we discuss this drastic change more quantitatively.

Closing this section, we comment on the applicability of our method. The obtained dispersions are reliable only in low-energy part because of two principal reasons. First, since the energy dispersion are estimated by the single particle state (18), this method is effective only in the low-density limit. In other words, one cannot apply this method to high-field phenomena where the number of triplet particles is large so that many-body interactions between triplet ones become important. Second, because the state (18) has translational symmetry, one cannot explain magnetization plateau breaking the symmetry by this method.

#### IV. CRITICAL BEHAVIOR NEAR THE LOW-FIELD CUSP SINGULARITY

To discuss quantitatively the behavior of the magnetization curve near the cusp singularity, we consider field derivative of the magnetization  $dm/dh$ .

From Eq.(21), we find that  $dm/dh$  is given by the density of states at the Fermi energy

$$\begin{aligned} \frac{dm}{dh} &= \frac{1}{2\pi} \int_0^{2\pi} \delta(h - \omega(k)) dk \\ &= \frac{L}{2\pi} \sum_{\{\omega(k)=h\}} \left| \frac{d\omega(k)}{dk} \right|^{-1}, \end{aligned} \quad (22)$$

where  $\sum_{\{\omega(k)=h\}}$  indicates a sum over all Fermi points. In the case of the double-bottom shape dispersion, two different situations may occur (see Fig.3(a)).

[1] For  $h > h_{\text{cusp}}$ , there are two Fermi points  $\pm k_F$ , and the energy band can be linearized around the fermi points as far as low-energy excitations are concerned:  $\omega(k) = \pm v_F \{(k - \pi) \mp k_F\}$ , where  $v_F$  is the Fermi velocity of the  $t_+$  fermions. Thus, from Eq.(22), we obtain  $dm/dh = L/\pi v_F$  which is almost independent of  $h$  because  $v_F$  only depends weakly on  $h$ .

[2] For  $h < h_{\text{cusp}}$ , there are four Fermi points satisfying the relation  $2k_{F1} - 2k_{F2} = m$ . In this case, low-

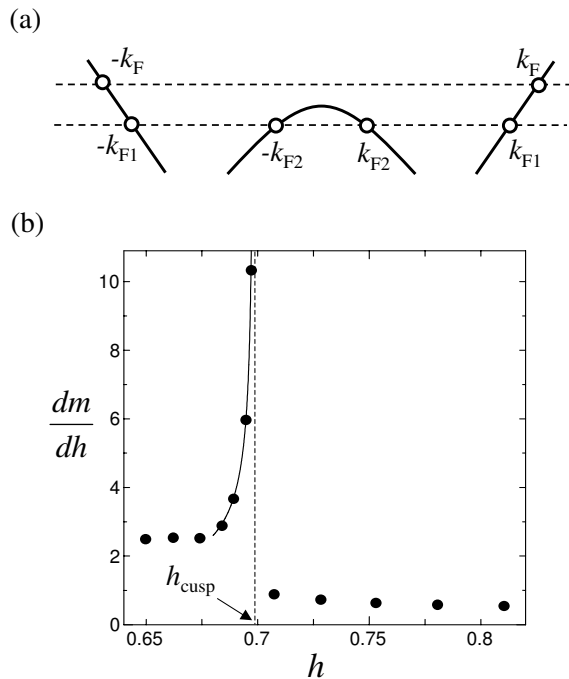


FIG. 3: (a) The effective low-energy dispersion and (b) the field derivative of the magnetization  $dm/dh$  near  $h = h_{\text{cusp}}$  of the frustrated Kondo necklace model with  $J = J_K$  and  $\lambda = 0.5$ . The solid line denotes asymptotic curve  $dm/dh \sim (h_{\text{cusp}} - h)^{-1/2}$  near  $h = h_{\text{cusp}}$ .

energy states are effectively described by following two-band model [see Fig3(a)].

$$\omega_1(k) = \pm v_{F1} \{ (k - \pi) \mp k_{F1} \}, \quad (23)$$

$$\omega_2(k) = -c(k - \pi)^2 + h_{\text{cusp}}. \quad (24)$$

The parabolic dependence of  $\omega_2(k)$  around  $k = \pi$  gives decisive difference in  $dm/dh$  from the case [1]. Using Eq.(24) in Eq.(22), we obtain the most dominant contribution

$$\frac{dm}{dh} \sim \frac{L}{2\pi\sqrt{c}} \frac{1}{\sqrt{h_{\text{cusp}} - h}} \quad (25)$$

which diverges at  $h = h_{\text{cusp}}$ . Thus, we find that the critical exponent is given by  $\gamma = 1/2$ .

Plots in Fig.3(b) show the field derivative of the magnetization  $dm/dh$  of our model (1) with  $J = J_K$  and  $\lambda = 0.5$  obtained by differentiating numerically the DMRG data in Fig.1. As shown by the above results, for  $h > h_{\text{cusp}}$ , the plots are almost independent of the magnetic field. On the other hand, for  $h < h_{\text{cusp}}$ , it diverges as  $dm/dh \sim (h_{\text{cusp}} - h)^{-1/2}$  as  $h \rightarrow h_{\text{cusp}}$  (the solid line in Fig.3(b)). Away from the cusp singularity  $h_{\text{cusp}}$ , the data are almost independent of  $h$ . This means that the low-energy dispersion is described by two linear-bands involving four Fermi points.

From the above results, we find that the magnetization

behaves as

$$m - m_{\text{cusp}} \propto \begin{cases} h - h_{\text{cusp}} & : h > h_{\text{cusp}} \\ -\sqrt{h_{\text{cusp}} - h} & : h < h_{\text{cusp}} \end{cases} \quad (26)$$

near the critical point  $h = h_{\text{cusp}}$ . This result well explains the behavior of magnetization curves near  $h = h_{\text{cusp}}$  obtained by our DMRG calculations (see Fig.1).

## V. PHASE DIAGRAM

As we saw in the previous section, when the frustration parameter  $\lambda$  is large, the value of the energy dispersion at  $k = \pi$  changes into local maximum from minimum at certain critical  $\lambda_c$ . Therefore, the critical points  $\lambda_c$  can be determined by the condition that second derivative of the energy dispersion at  $k = \pi$  vanish:

$$\left( \frac{\partial^2 \omega(k)}{\partial k^2} \right)_{k=\pi} = 0. \quad (27)$$

For  $\lambda < \lambda_c$  (no cusp phase),  $(\partial^2 \omega / \partial k^2)_{k=\pi}$  is positive and the Kondo singlet gap  $\Delta_K$  takes its minimum value at  $k = \pi$ . In the region where the gap  $\Delta_K$  collapses, the system belongs to a conventional one-component Tomonaga-Luttinger (TL) liquid phase. [15, 16] On the other hand, for  $\lambda > \lambda_c$  (cusp phase),  $(\partial^2 \omega / \partial k^2)_{k=\pi}$  is negative and the position of the minimum gap moves away from  $k = \pi$ . In this case, the system exhibits a two-component TL liquid [30] characterized by two differential Fermi velocities when the Fermi energy  $h$  is positioned between the gap  $\Delta_K$  and the local maximum at  $k = \pi$ .

In this section, we determine the phase boundary on  $J$ - $\lambda$  plane separating two TL liquid phases as mentioned above. First, we discuss the phase boundary in the strong Kondo-coupling region  $J \ll J_K = 1$  making use of the results in previous section. The Taylor expansion of Eq.(20) around  $k = \pi$  is given as

$$\omega(k) = \Delta_K + \frac{\alpha}{2!}(k - \pi)^2 + \frac{\beta}{4!}(k - \pi)^4 + \dots, \quad (28)$$

where the coefficients  $\Delta_K$ ,  $\alpha$  and  $\beta$  are given by

$$\Delta_K = 1 - \frac{1}{2}J + \frac{\lambda}{4}J [2 + (1 + \lambda)J], \quad (29)$$

$$\alpha = J \left( 2 + \frac{5}{4}J \right) \left( \lambda - \frac{2 + 2J}{8 + 5J} \right), \quad (30)$$

$$\beta = J \left[ \frac{1}{2} + 8\lambda - 12 \left( \lambda^2 - \frac{5}{6}\lambda + \frac{1}{16} \right) J \right]. \quad (31)$$

Thus, imposing the condition (27), we obtain the boundary line on the  $J$ - $\lambda$  plane:

$$\lambda_c = \frac{2 + 2J}{8 + 5J} \quad (32)$$

in the strong Kondo-coupling region. Beyond the strong Kondo-coupling region, however, this result is not valid.

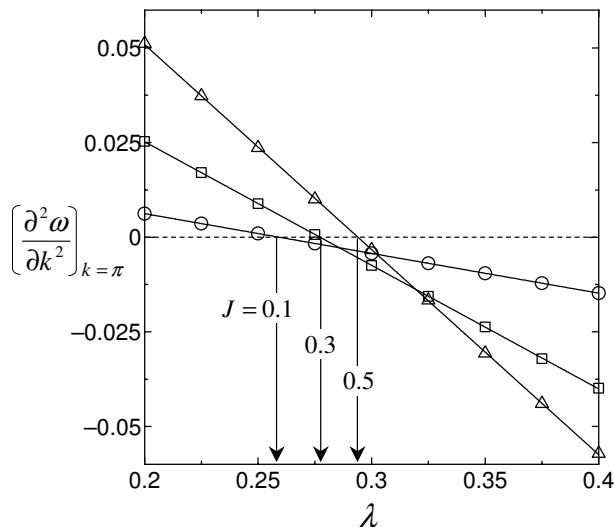


FIG. 4: The second derivative of the energy dispersion  $\omega$  at  $k = \pi$ . The circles, squares and triangles denote  $(\partial^2\omega/\partial k^2)_{k=\pi}$  for  $J = 0.1, 0.3$  and  $0.5$  respectively. Each symbol is fitted by a straight line.

We therefore determine the critical point  $\lambda_c$  from the energy dispersion calculated by the exact-diagonalization method. We fit the exact-diagonalization data near  $k = \pi$  using the form (28) up to eighth order and estimate fitting parameters  $\Delta_K, \alpha, \beta, \dots$  for various  $\lambda$  on fixed  $J$ . The obtained  $\alpha = (\partial^2\omega/\partial k^2)_{k=\pi}$  for  $J = 0.1, 0.3$  and  $0.5$  are shown by circles, squares and triangles in Fig.4, respectively. The next step is to interpolate  $\alpha$  to obtain the critical point  $\lambda_c$  that satisfies the condition (27). As the interpolation function, we assume a linear function  $\alpha = A(\lambda - \lambda_c)$  on the analogy of the strong Kondo-coupling form Eq.(30). Thus, we can obtain the critical point  $\lambda_c$  from the condition  $\alpha = 0$  (see Fig.4). Finally, the phase diagram on  $J$ - $\lambda$  plane is constructed by performing a series of procedure for various values of  $J$ , as Fig.5. The short-dash line in Fig.5 shows the boundary given by Eq.(32) in the strong Kondo-coupling limit. On the boundary, the magnetization curve grows rapidly at  $h = \Delta_K$  because the low-energy part of the dispersion becomes quartic. More explicitly, from Eq.(22), the magnetization behaves  $m \sim (h - \Delta_K)^{3/4}$ .

## VI. SUMMARY AND DISCUSSION

In this paper, we present a detailed study of magnetization process of the frustrated Kondo necklace model. From the DMRG calculations based on finite-size algorithm, we observed two plateaus and two cusp singularities in the magnetization curve. The magnetization plateaus at zero ( $m = 0$ ) and at a half saturation magnetization ( $m = 1/2$ ) were previously found by numerical exact-diagonalization, and these mechanisms were well

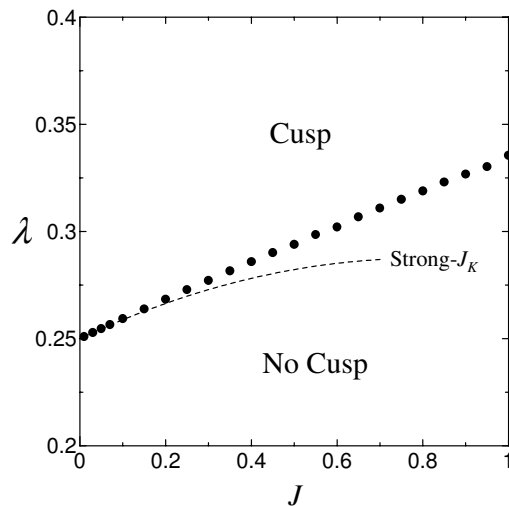


FIG. 5: The phase diagram on  $J$ - $\lambda$  plane which decides whether a cusp appears in the region of  $0 < m < 1/2$  in the magnetization curve. The short-dash line is the boundary given by Eq.(32) obtained from the strong Kondo-coupling expansion up to second order.

understood [14, 15, 16]. The two magnetization cusps appears in the low-field ( $0 < m < 1/2$ ) and high-field ( $1/2 < m < 1$ ) regions respectively. Among these two cusps, although the high-field cusp was expected from the PWFRG study of the spin-1/2 zig-zag ladder by Okunishi et al, the low-field cusp was unexpected. We therefore paid attention to the low-field cusp and discussed its mechanism using the strong Kondo-coupling expansion as well as numerical diagonalization method. To explain the appearance of the cusp in term of fermionic band picture, we expressed the original spin Hamiltonian (1) in terms of the fermionic bond-operators, and obtained the energy dispersion by assuming the single triplet state (18). Also, since the obtained dispersions were in good agreement with the numerical diagonalization data, we conclude that the low-energy physics of the present model with strong Kondo-coupling are well described by the single triplet state (18). When the frustration parameter  $\lambda$  is large, the shape of the energy dispersion varies from a single bottom to double bottoms. In the case of the double-bottom shape, the increase ratio of the  $t_+$  particle number drastically changes when the Fermi energy (the external magnetic field  $h$ ) reaches the local maximum at  $k = \pi$ . The appearance of the cusp singularity can be explained by this drastic change. We also discussed the critical behavior of the magnetization near the cusp singularity point. We found that  $dm/dh \propto (h - h_{\text{cusp}})^{-1/2}$  ( $h < h_{\text{cusp}}$ ) and  $dm/dh \sim \text{const.}$  ( $h > h_{\text{cusp}}$ ). Moreover, we obtained the phase diagram on the  $J$ - $\lambda$  plane that decides whether the cusp appears in the magnetization curve. In the cusp phase, when the Fermi energy  $h$  lies between the Kondo singlet gap  $\Delta_K$  and the local maximum at  $k = \pi$ , the system exhibits a two-component TL

liquid characterized by two different Fermi velocities. On the other hand, in the no-cusp phase, the conventional one-component TL liquid phase is stabilized in the region  $\Delta_K < h < h_S$ . At  $h = \Delta_K$ , the phase boundary on the  $J$ - $\lambda$  plane corresponds to the critical line separating the one-component and the two-component TL liquids.

Recently, Fath and Littlewood [8, 9] showed the existence of the transition between above-mentioned two TL liquid phases when the Haldane gap collapses in the spin-1 bilinear-biquadratic chain. They also mentioned that there is another critical (Lifshitz) point where the incommensurability manifests itself in the static structure factor. Their result brings us an interesting question whether or not such a Lifshitz point is present in our model. It is beyond the scope of this paper and remained as our future work.

## Acknowledgments

We are grateful to M. Asano for his assistance in the DMRG calculation. We also would like to thank Prof. C. Ishii and T. Nikuni for making a number of useful discussions and critical reading of manuscript. We learned much about the exact-diagonalization method based on Lanczos algorithm from the program TITPACK version 2 developed by H. Nishimori at Tokyo Institute of Technology.

The work has been supported in part by Frontier Research Center for Computational Science (FRCCS) of Tokyo University of Science.

- 
- [1] M. Oshikawa, M. Yamanaka, and I. Affleck, Phys. Rev. Lett. **78**, 1984 (1997).
  - [2] W. Shiramura, K. Takatsu, B. Kurniawan, H. Tanaka, H. Uekusa, Y. Ohashi, K. Takizawa, H. Mitamura, and T. Goto, J. Phys. Soc. Jpn. **67**, 1548 (1998).
  - [3] H. Kageyama, K. Yoshimura, R. Stern, N. V. Mushnikov, K. Onizuka, M. Kato, K. Kosuge, C. P. Slichter, T. Goto, and Y. Ueda, Phys. Rev. Lett. **82**, 3168 (1999).
  - [4] M. Ishii, H. Tanaka, M. Hori, H. Uekusa, Y. Ohashi, K. Tatani, Y. Narumi and K. Kindo, J. Phys. Soc. Jpn. **69**, 340 (2000).
  - [5] T. Goto, M. I. Bartashevich, Y. Hosokoshi, K. Kato and K. Inoue, Physica B **294-295**, 43 (2001).
  - [6] H. Tanaka, T. Ono, H. A. Katori, H. Mitamura, F. Ishikawa, T. Goto, cond-mat/0204125, will appear in Supplement of Progress in Theoretical Physics
  - [7] M. Fujii, S. Fujimoto and N. Kawakami, J. Phys. Soc. Jpn. **65**, 2381 (1996).
  - [8] G. Fath and P. B. Littlewood, Phys. Rev. B **58**, R14709 (1998)
  - [9] G. Fath and A. Suto, Phys. Rev. B **62**, 3778 (2000)
  - [10] K. Okunishi, Y. Hieida, and Y. Akutsu, Phys. Rev. B **60**, R6953 (2000).
  - [11] K. Okunishi and N. Maeshima, Phys. Rev. B **64**, 212406 (2001).
  - [12] C. Gerhardt, K.-H. Mutter, and H. Kroger, Phys. Rev. B **57**, 11504 (1998).
  - [13] S. Hirata, cond-mat/9912066.
  - [14] T. Yamamoto, M. Asano, and C. Ishii, J. Phys. Soc. Jpn. **70**, 3678 (2001).
  - [15] T. Yamamoto and C. Ishii, to be published in Prog. Theor. Phys. Supp. No. 145, (2002).
  - [16] T. Yamamoto, K. Ide, and C. Ishii, cond-mat/0204174.
  - [17] J. Igarashi, T. Tonegawa, M. Kaburagi, and P. Flude, Phys. Rev. B **51**, 5814 (1995).
  - [18] S. Doniach, Physica B **91**, 231 (1977).
  - [19] G. -M. Zhang, Q. Gu, and L. Yu, Phys. Rev. B **62**, 69 (2000).
  - [20] R. T. Scalettar, D. J. Scalapino, and R. L. Sugar, Phys. Rev. B **31**, 7316 (1985).
  - [21] S. Moukouri, L. G. Caron, C. Bourbonnais, and L. Hubert, Phys. Rev. B **51**, 15920 (1994).
  - [22] H. Otsuka and T. Nishino, Phys. Rev. B **52**, 15066 (1995).
  - [23] Y. Chen, Q. Yuan, H. Chen, and Y. Zhang, Phys. Lett. A **245**, 167 (1998).
  - [24] S. R. White, Phys. Rev. Lett. **69**, 2863 (1992); Phys. Rev. B **48**, 10345 (1993).
  - [25] S. Sachdev and R. N. Bhatt, Phys. Rev. B **41**, 9323 (1990)
  - [26] S. Gopalan, T. M. Rice, and M. Sigrist, Phys. Rev. B **49**, 8901 (1993)
  - [27] Y. Matsushita, M. P. Gelfand, and C. Ishii, J. Phys. Soc. Jpn. **68**, 247 (1999).
  - [28] H.-T. Wang, H. Q. Lin and J.-L. Shen, Phys. Rev. B **61**, 4019 (2000).
  - [29] T. Barnes, E. Dagotto, J. Riera, and E. S. Swanson, Phys. Rev. B **47** 3196 (1993).
  - [30] M. Fabrizio, Phys. Rev. B **54**, 10054 (1996); *ibid.* **48**, 15838 (1993).